

INVESTIGATION OF THE CASCADES IN ATOMS USING THE GLOBAL CHARACTERISTICS OF SPECTRA

R. Karazija, S. Kučas, and V. Jonauskas

Vilnius University Research Institute of Theoretical Physics and Astronomy, A. Goštauto 12, LT-01108 Vilnius, Lithuania

Received 30 April 2004

Dedicated to the 100th anniversary of Professor A. Jucys

Following the creation of inner-shell vacancy in an atom, the cascade of radiative and nonradiative transitions takes place. It can be analysed employing the final charge distribution of ions, the electron and characteristic emission spectra. The development of the experimental and theoretical investigation of cascades is shortly reviewed. The main attention is paid to the description of a cascade using the global characteristics of spectra, especially in the cases of transitions between close-lying and overlapping configurations. Some applications of the global characteristics method are given.

Keywords: cascade, Auger cascade, highly charged ions, global characteristics

PACS: 32.80.Hd, 31.10.+z, 32.30.Rj

1. Introduction

One of the perspective directions in the inner-shell physics is the investigation of the cascades of elementary processes in atoms and of various spectra excited in such a way. It enables considering the specific features of inner electronic shells, the dynamics of the decay of highly excited states, the anomalous population of some configurations.

Such cascades start after the creation of one or several vacancies in the inner shells of an atom. During the radiative transition a vacancy is shifted from one electronic shell to another. As a result of the nonradiative Auger transition, two vacancies appear, thus the charge of the ion increases. At the effective nuclear charge $Z^{\text{eff}} \leq 30$ the Auger transitions are the dominating way of deexcitation (if they are not forbidden energetically). Only the innermost vacancies in the heavy atoms decay mainly by the radiative transitions. Thus, the role of Auger transitions increases during the cascade. At the fluorescence yield $\omega \approx 10^{-2} - 10^{-3}$ the contribution of radiative transitions can be practically neglected and the cascade is considered only as an Auger cascade. Due to the energetic constraints for Auger transitions their different paths end at different ionization stages, therefore, ions with various charges are obtained. The many-electron transitions during the excitation and the processes that

follow also increase a number of ions with the higher charge.

The first measurements of the charge state distributions were made for the vacancies created by the nuclear processes – electron capture and internal conversion in the radioactive isotopes of rare gases [1, 2]. The charge spectrometry was used for this purpose. In the middle of the sixties, a magnetic mass spectrometer was applied to detect photoions of various charges following irradiation of atomic gases by X-rays [3–6].

The accuracy of measurements essentially increased, when monochromatized synchrotron radiation was used to prepare the initial state with inner vacancies and the time-of-flight mass spectrometer to detect ions [7–9]. By changing the wavelength of the radiation in a certain interval, the photoion-yield spectra are recorded [8]. They give the dependence of the intensities of various ions on the photon energy. The more refined data are obtained when using the coincidence technique [10–16]. The photoelectron–photoion coincidence experiment enables one to separate the charge state distribution corresponding to the creation of a vacancy in a given subshell. The Auger electron–photoion coincidence measurements specify the Auger transitions for various multiply charged ions.

Very complicated cascades take place after atom–ion collisions [17–19]. The specific case is the cascades in the hollow atoms, created in collision processes be-

tween highly charged ions and solid surfaces or other targets [20–22].

Cascades involve many configurations with several open shells, such configurations have thousands and millions of levels. Thus, the detailed level-by-level calculations of a cascade are very complicated and practically possible only for light atoms or for the initial vacancies in subvalent shells. On performing such calculations the theory of many-electron atom with several open shells must be used. It is necessary to note that considerable contribution to the development of such theory was given by the works of A. Jucys [23–25], to whose centenary this collection of papers is devoted.

As far as we know, the first detailed calculation of the Auger cascade was performed for Al in [26] and the theoretical analysis of the emission spectrum taking into account the population of levels by a cascade of processes in [27]. Up to now such calculations even for the main part of the cascade are not numerous: in such a way the radiative decay of vacancies in subvalent shells of Kr [28], the Auger transitions following deep core ionization in Ar [29, 30], the $3d_{5/2} - 5p$ excitation in Kr and $4d_{5/2} - 6p$ in Xe [31], the $3d$ ionization in Xe [32] are studied.

The natural width of the lines corresponding to the transitions between configurations with inner vacancies exceeds the energetic distances between the lines in complex spectra. Then the separate lines coalesce into broad maxima and the detailed calculation of the cascade is even inexpedient, at least of its all processes.

Two theoretical methods were proposed for the approximate description of a cascade: the statistical Monte Carlo simulation and the construction of deexcitation tree using the global characteristics of spectra (its earliest simpler variant is the average configuration method).

The Monte Carlo method is based on the accidental choice of the deexcitation path development with the account for the relative probabilities of various transitions. Such simulation is repeated about 10^5 times and the final distribution of vacancies or charge distribution of the ions is found. Already in the first applications of this method [3–6] not only the radiative and Auger transitions, but also many-electron transitions in the shake-off model were taken into account. During the development of the cascade some of the Auger transitions became energy forbidden: it was checked in [33] by computing the average energies equal to the differences of the average energies of initial and final configurations. The Monte Carlo method did not gain much popularity [34–36], because it required more computation time

than the average configuration method. By applying the latter method, the cascade is calculated only once using the same atomic data.

The average configuration method for the investigation of cascades was elaborated in [37]. The main idea of this method is to calculate the development of the cascade considering the transitions between vacancy states or configurations with the rate equal to the total transition rate and energy equal to the difference of the average energies of configurations. It was proposed in [28] to apply this method for the preliminary analysis of the cascade, to determine its main part, giving the essential contribution to the considered emission or Auger spectrum, and then to perform the detailed calculations of the main processes.

The total transition rate and the average energy of configuration are the simplest global characteristics of spectra. Using such other characteristics and taking into account the distribution of intensities in the spectra (characteristics of zones, variance of spectra etc.) the more accurate description of the cascade and its effects on the spectra can be obtained. The algebraic expressions for the main global characteristics of energy level [38–40], emission [38, 41], and Auger [42] spectra are known. For the derivation of these characteristics the general group diagrammatic method was elaborated [43–45].

The method of global characteristics is very useful for the description of transitions between close-lying or overlapping configurations. On using the density of states the coefficient for the diminishing of transition rate for overlapping configurations was introduced [46]. More accurately such transitions can be described in the terms of zones of configurations and their global characteristics [47, 48].

The preferable object for the study of cascades are inert gas atoms. The charge state and photoion spectra were studied for Ne [3, 49], Ar [4, 11, 12, 50–53], Kr [5, 6, 33, 53–56], Xe [6, 9, 16, 34, 35, 46, 57–60], and for all of them [61–63]. Also such spectra were investigated for lanthanides [7–9, 15, 32, 64–66], Mg [50, 67], Al, Si, S, Ca, Fe [50], Cu [18], Sr [68], Ba [69], Au [70], Re [71], and Ta [71]. In [36] the ion charge distribution due to vacancy cascades following the K , L_1 , L_2 , and L_3 shell ionization were calculated by the Monte Carlo method for the atomic numbers $Z = 10–60$. The Auger cascade spectra were mostly studied for Ar [13, 29, 30, 72–77]; also several works were devoted to Kr [31, 73], Xe [31, 32, 78], Al [26], Ni [79], and Eu [66]. Because the X-ray transitions accompanying the cascade decay of inner-shell vacancies are

less probable than the Auger transitions, the cascade affected emission spectra are less investigated, the results are mainly obtained for inert gases [27, 33, 80–84] as well as for Fe [37], Ag [80], and Pb, Th, U [85]. During the last years some angle resolved studies of the Auger cascades following photoexcitation from an inner shell were performed for Ar, Kr, and Xe [31, 86–89].

The following sections of this work are devoted to the averaged description of the elementary processes proceeding during the cascade (Section 2), consideration of transitions between close-lying and overlapping configurations (Section 3), and some applications of the global characteristics method (Section 4).

2. Elementary processes following the cascade and their averaged description

Intensities of the spectral lines depend not only on the probabilities of the corresponding transitions, but also on the populations of initial levels. At the dynamical equilibrium of the system (the number of atoms excited to a given level is equal to the number of atoms deexcited from this level at the same time) the population of the level γ of configuration K is expressed as [90]

$$N(K\gamma) = \frac{\sum_{K'\gamma'} N(K'\gamma') \sum_s A_s(K'\gamma' - K\gamma)}{A(K\gamma)}, \quad (1)$$

where $A_s(K'\gamma' - K\gamma)$ is the rate of the transition from the level γ' of configuration K' to the level γ of configuration K by the process s , $A(K\gamma)$ is the total deexcitation rate of the level γ :

$$A(K\gamma) = \sum_s \sum_{K'\gamma'} A_s(K\gamma - K'\gamma'). \quad (2)$$

The main idea of the averaged configuration method is to consider the transitions not between the separate levels, but between the configurations. Then Eqs. (1), (2) are replaced by

$$N(K) = \frac{\sum_{K'} N(K') \sum_s A_s(K' - K)}{A(K)}, \quad (3)$$

$$A(K) = \sum_s \sum_{K'} A_s(K - K'). \quad (4)$$

Here $A_s(K' - K)$ is the total rate of transitions between all levels of configurations K and K' :

$$A_s(K - K') = \sum_{\gamma\gamma'} A_s(K\gamma - K'\gamma'). \quad (5)$$

On the usual assumption that the radial orbitals of electrons do not depend on many-electron quantum numbers, the summation in Eq. (5) can be performed algebraically.

The radiative transition rate is expressed in terms of the line strength and the transition energy in a certain power. The dependence of the rate on many-electron quantum numbers is mainly determined by the line strength. The dependence of the transition energy, especially in the case of transitions between the inner shells, is considerably weaker. Thus, for the approximate calculation of cascades it can be replaced by the average energy of the transition array between two configurations. Its simplest expression is the difference of the average energies of the initial and final configurations

$$\bar{E}(K - K') \approx \bar{E}(K) - \bar{E}(K'). \quad (6)$$

A more exact expression is obtained by averaging the transition energy with the weight equal to its line strength $S(K\gamma, K'\gamma')$:

$$\begin{aligned} \bar{E}(K - K') = & \\ & \frac{\sum_{\gamma\gamma'} [\langle K\gamma | H | K\gamma \rangle - \langle K'\gamma' | H | K'\gamma' \rangle] S(K\gamma, K'\gamma')}{\sum_{\gamma\gamma'} S(K\gamma, K'\gamma')}. \end{aligned} \quad (7)$$

It is expressed by the difference $\bar{E}(K) - \bar{E}(K')$ and the shift due to the distribution of lines in the spectrum:

$$\bar{E}(K - K') = \bar{E}(K) - \bar{E}(K') + \delta\bar{E}(K - K'). \quad (8)$$

In the nonrelativistic approximation this shift is described by the formula [38]

$$\begin{aligned} \delta\bar{E}(K_0 n_1 l_1^{N_1} n_2 l_2^{N_2} - K_0 n_1 l_1^{N_1+1} n_2 l_2^{N_2-1}) & \\ = \frac{1}{(4l_1 + 1)(4l_2 + 1)} & \\ \times \sum_{k>0} \begin{Bmatrix} l_1 & l_1 & k \\ l_2 & l_2 & 1 \end{Bmatrix} \langle l_1 || C^{(k)} || l_1 \rangle \langle l_2 || C^{(k)} || l_2 \rangle & \\ \times [-N_1(4l_2 + 2 - N_2) F_K^k(n_1 l_1, n_2 l_2) & \\ + (4l_1 + 1 - N_1)(N_2 - 1) F_{K'}^k(n_1 l_1, n_2 l_2)] & \\ + \frac{1}{(4l_1 + 1)(4l_2 + 1)} & \\ \times \sum_k (-1)^k \left[\frac{2}{3} \delta(k, 1) - \frac{1}{2(2l_1 + 1)(2l_2 + 1)} \right] & \end{aligned}$$

$$\begin{aligned} & \times \langle l_1 \| C^{(k)} \| l_2 \rangle^2 \\ & \times [-N_1(4l_2 + 2 - N_2)G_K^k(n_1l_1, n_2l_2) \\ & + (4l_1 + 1 - N_1)(N_2 - 1)G_{K'}^k(n_1l_1, n_2l_2)]. \quad (9) \end{aligned}$$

Here K_0 means all passive open or closed shells not involved in the transitions, N_i is the number of electrons in the i th shell, $\langle l_1 \| C^{(k)} \| l_2 \rangle$ is the reduced matrix element of the spherical function, and F^k , G^k are the Coulomb integrals calculated with the radial wave functions of the configuration indicated as a subscript.

A more complicated expression for this shift is obtained in the relativistic approximation [91]. The simpler way to account for the relativistic effects is to replace the nonrelativistic integrals in Eq. (9) by the corresponding linear combinations of relativistic integrals. The explicit expression for the total line strength of radiative transitions between two configurations has the form

$$\begin{aligned} & S(K_0\lambda_1^{N_1}\lambda_2^{N_2}, K_0\lambda_1^{N_1+1}\lambda_2^{N_2-1}) \\ & = g(K_0) \binom{\Omega_1 - 1}{N_1} \binom{\Omega_2 - 1}{N_2 - 1} \langle \lambda_1 \| o \| \lambda_2 \rangle^2. \quad (10) \end{aligned}$$

Here λ_i means the quantum numbers of the shell $n_i l_i$ or the subshell $n_i l_i j_i$, Ω_i is the number of single-electron states in the shell ($4l_i + 2$) or the subshell ($2j_i + 1$), $g(K_0)$ is the statistical weight of the passive shells (subshells) that do not take part in the transitions, $\binom{a}{b}$ is the number of combinations. Equation (10) holds for any radiative transition operator of every multiplicity in nonrelativistic or relativistic approximation. This specific feature of the operator holds only in its one-electron reduced matrix element. In the nonrelativistic approximation for the main electric dipole transitions it equals to

$$\langle n_1 l_1 s \| o^{(1)} \| n_2 l_2 s \rangle = \sqrt{2} \langle l_1 \| C^{(1)} \| l_2 \rangle \langle n_1 l_1 | r | n_2 l_2 \rangle. \quad (11)$$

The multiplier $\sqrt{2}$ appears due to the scalarity of the operator in the spin space. The formulae for the matrix elements of electric and magnetic transitions in the relativistic approximation are given, for example, in [92, 93].

The Auger transition rate does not depend explicitly on the transition energy, thus the line strength is not introduced and the total transition rate is used. For the two main types of Auger transitions the following expressions are obtained [90, 94]:

$$\begin{aligned} & A(K_0\lambda_1^{N_1}\lambda_2^{N_2} \rightarrow K_0\lambda_1^{N_1+1}\lambda_2^{N_2-2}\varepsilon\lambda) \\ & = g(K_0) \binom{\Omega_1 - 1}{N_1} \binom{\Omega_2 - 2}{N_2 - 2} A(\lambda_2^2 - \lambda_1\varepsilon\lambda), \quad (12) \end{aligned}$$

$$\begin{aligned} & A(K_0\lambda_1^{N_1}\lambda_2^{N_2}\lambda_3^{N_3} \rightarrow K_0\lambda_1^{N_1+1}\lambda_2^{N_2-1}\lambda_3^{N_3-1}\varepsilon\lambda) \\ & = g(K_0) \binom{\Omega_1 - 1}{N_1} \binom{\Omega_2 - 1}{N_2 - 1} \binom{\Omega_3 - 1}{N_3 - 1} \\ & \quad \times A(\lambda_2\lambda_3 - \lambda_1\varepsilon\lambda). \quad (13) \end{aligned}$$

Here λ_i , Ω_i , and $g(K_0)$ have the same meaning as in Eq. (10), λ means the quantum numbers of the Auger electron l or lj . Because the summation over λ cannot be accomplished explicitly, the expressions are given for the Auger channel. The last multiplier in the right-hand side of Eqs. (12), (13) is the Auger transition rate in the two-electron model. It is expressed by the sum of two-electron matrix elements of the operator h responsible for the autoionization transitions (atomic units are used):

$$A(\lambda_2\lambda_3 - \lambda_1\varepsilon\lambda) = \sum_{\Lambda} \langle \lambda_2\lambda_3\Lambda \| h \| \lambda_1\varepsilon\Lambda \rangle^2, \quad (14)$$

where Λ means LS in LS -coupling and J in jj -coupling. In the nonrelativistic approximation h is usually approximated by the operator of Coulomb interaction between electrons. Then in the case of LS -coupling within shells we have:

$$\begin{aligned} & A(n_2l_2, n_3l_3 - n_1l_1\varepsilon l) \\ & = 4 \sum_k \left\{ \frac{1}{2k+1} \langle l_1 \| C^{(k)} \| l_2 \rangle^2 \langle l \| C^{(k)} \| l_3 \rangle^2 \right. \\ & \quad \times R^k(n_2l_2n_3l_3, n_1l_1\varepsilon l)^2 \\ & \quad + \frac{1}{2k+1} \langle l_2 \| C^{(k)} \| l \rangle^2 \langle l_1 \| C^{(k)} \| l_3 \rangle^2 \\ & \quad \times R^k(n_2l_2n_3l_3, \varepsilon l n_1l_1)^2 \\ & \quad - \sum_{k'} (-1)^{k+k'} \langle l_2 \| C^{(k)} \| l_1 \rangle \langle l_3 \| C^{(k)} \| l \rangle \\ & \quad \times \langle l_2 \| C^{(k')} \| l \rangle \langle l_3 \| C^{(k')} \| l_1 \rangle \left. \left\{ \begin{matrix} l_1 & l_2 & k \\ l & l_3 & k' \end{matrix} \right\} \right\} \\ & \quad \times R^k(n_2l_2n_3l_3, n_1l_1\varepsilon l) R^{k'}(n_2l_2n_3l_3, \varepsilon l n_1l_1) \Big\}, \quad (15) \end{aligned}$$

$$A(n_2 l_2^2 - n_1 l_1 \varepsilon l) = \frac{1}{2} \delta(n_2, n_3) \delta(l_2, l_3) A(n_2 l_2, n_3 l_3 - n_1 l_1 \varepsilon l). \quad (16)$$

Here R^k is the general integral of Coulomb interaction.

In the relativistic approximation the Breit operator or some of its terms are taken into account in addition to the Coulomb interaction operator. The formulae for the two-electron matrix elements are given, for example, in [92, 93], and their direct summation can be accomplished easily. The total line strength of radiative transitions (10) and the total Auger transition rate (12), (13) consist of the statistical multipliers, depending on the numbers of electrons in the active shells or subshells, and of the one- or two-electron quantities, depending only on the radial orbitals of these electrons. It enables the extrapolation of the global characteristics for the other transitions between the same shells (subshells) of the same element as well as for the same transitions in the atoms of different elements.

For the analysis of a cascade only the relative populations of configurations are needed. Thus, if the cascade begins only from one excited configuration, its population can be taken equal to 1. If during the excitation process several excited configurations are created, their relative populations must be calculated using the total excitation probabilities or cross-sections. Usually atoms are excited from one ground level. The cross-sections of photoionization and photoexcitation as well as of the excitation or ionization by electron beam in the first Born approximation of plane waves are expressed in terms of the line strength of multipole transitions.

If the initial vacancy is created by photoexcitation from the closed inner shell or subshell, the sum over all levels of the final configuration divided by the statistical weight $g_\gamma = 2J + 1$ of the initial level γ yields a simple expression independent of many-electron quantum numbers of the initial level:

$$\frac{1}{g_\gamma} \sum_{\gamma_2 \gamma'} S(K_0 \lambda_1^{\Omega_1} \lambda_2^{N_2} \gamma_2 \gamma, K_0 \lambda_1^{\Omega_1-1} \lambda_2^{N_2+1} \gamma_2' \gamma') = \frac{\Omega_2 - N_2}{\Omega_2} \langle \lambda_1 || o || \lambda_2 \rangle^2. \quad (17)$$

By substituting $\lambda_2 \rightarrow \varepsilon \lambda$ at $N_2 = 0$ and separating one open shell (subshell) from K_0 we obtain the expression

for the ionization from a closed shell in the presence of an open shell:

$$\frac{1}{g_\gamma} \sum_{\gamma_2 \gamma'} S(K_0 \lambda_1^{\Omega_1} \lambda_2^{N_2} \gamma_2 \gamma, K_0 \lambda_1^{\Omega_1-1} \lambda_2^{N_2} \gamma_2' \varepsilon \lambda \gamma') = \langle \lambda_1 || o || \varepsilon \lambda \rangle^2. \quad (18)$$

Here K_0 can also contain the other open shells.

The population of the initial configuration by the inner shell ionization with electron beam is described by the average collisional ionization strength. Its formula is given in [95].

During the initial excitation of an atom and the subsequent radiative or Auger decay, described by p -electron transition operators, the $(p+1)$ -electron processes also play a significant role. For the investigation of cascades they are usually calculated in the sudden perturbation approximation. The sudden change of the potential caused by the production of a vacancy or by its shift from one shell to another can excite the additional electron (shake-up) or remove it from the atom (shake-off). These transitions involving excited electrons are less probable and such weakly bound electrons usually are shaken off during future decay, thus all the probability to remove the electron during the sudden perturbation approximately can be attributed to the shake-off effect [3, 46]. The probability to remove an additional electron from the nl^N -shell is approximately expressed in terms of the overlap integral between the radial orbital $P_{nl}(r)$ before and after the perturbation:

$$A(nl^{-1}) = N [1 - \langle nl_K | nl_{K'} \rangle^2], \quad (19)$$

where K is the initial, and K' is the final configuration. The analogous formula holds for the expulsion of an electron from a subshell.

3. Transitions between close-lying and overlapping configurations. Zones of transitions

The most probable and thus rather important for the cascades are the transitions involving the neighbouring shells. The energy spectra of the initial and final configurations can even overlap, and transitions between some levels of such configurations become forbidden energetically. Then it is necessary to take into account the energetic intervals of configurations and the distribution of intensities in the spectrum.

The width of the energy level spectrum of configuration K can be approximately determined as a full

width at the half-maximum of the normal distribution of states:

$$\Delta E(K) = 2\sqrt{2 \ln 2} \sigma(K), \quad (20)$$

where $\sigma^2(K)$ is the variance of the distribution, $\sigma(K) = \sqrt{\sigma^2(K)}$.

The energy interval of the configuration spectrum is estimated as

$$\bar{E}(K) - \frac{\Delta E(K)}{2}, \quad \bar{E}(K) + \frac{\Delta E(K)}{2}. \quad (21)$$

The general formulae for the variance of the energy level spectrum in nonrelativistic and relativistic approximations were given in [38, 40].

In the case of transitions between overlapping configurations the total transition rate must be diminished by some coefficient. It can be calculated using the distribution functions of states [46]:

$$a = \int_{-\infty}^{\infty} \rho_K(E) \int_{-\infty}^E \rho_{K'}(E') dE dE', \quad (22)$$

where ρ_K and $\rho_{K'}$ are respectively the distribution functions for the initial and final configurations. For the description of cascades they can be approximated by the Gaussian function:

$$\rho(E) = \frac{1}{\sqrt{2\pi}\sigma} \exp\left(-\frac{E - \bar{E}(K)}{2\sigma^2(K)}\right)^2. \quad (23)$$

More accurately the transitions between close-lying configurations can be described introducing the zones of configurations taking into account the distribution of the line strengths or rates in the spectrum [47, 48].

The emissive zone characterizes the main part of the energy level spectrum of the initial configuration, involved in the considered transitions, and the receptive zone similarly describes the final configuration. These zones are determined by their moments.

For the radiative transitions between configurations K and K' the distribution moment of the k th order of the zone is obtained by averaging the k th power of the energy of the level of the initial or final configuration with the weight equal to the sum of the line strength from this level [47]:

$$\alpha_k^{\text{em}}(K) = \frac{\sum_{\gamma} \langle K\gamma | H | K\gamma \rangle^k \sum_{\gamma'} S(K\gamma, K'\gamma')}{\sum_{\gamma\gamma'} S(K\gamma, K'\gamma')}, \quad (24)$$

$$\alpha_k^{\text{rec}}(K') = \frac{\sum_{\gamma'} \langle K'\gamma' | H | K'\gamma' \rangle^k \sum_{\gamma} S(K\gamma, K'\gamma')}{\sum_{\gamma\gamma'} S(K\gamma, K'\gamma')}. \quad (25)$$

The sum in the denominator is the total line strength $S(K, K')$ (10). The sum of the line strengths over all levels of the final configuration is called the emissivity of the initial level; it is expressed by Eq. (17).

For the calculations of cascades only the first two moments of zones are necessary. The first moment is the average energy of zone:

$$\alpha_1(K) = \bar{\mathcal{E}}^{\text{em}}(K), \quad \alpha_1(K') = \bar{\mathcal{E}}^{\text{rec}}(K'). \quad (26)$$

The variance of the zone $\sigma^2(K)$ is expressed in terms of its first and second moments:

$$\sigma^2(K) = \alpha_2(K) - (\alpha_1(K))^2. \quad (27)$$

The shift of the average energy of a zone with respect to the average energy of a configuration for the transitions

$$K \equiv K_0 n_1 l_1^{N_1} n_2 l_2^{N_2} \rightarrow K' \equiv K_0 n_1 l_1^{N_1+1} n_2 l_2^{N_2-1} \quad (28)$$

can be expressed from Eqs. (7)–(9) and (24), (25):

$$\begin{aligned} \delta \mathcal{E}_{\text{rad}}^{\text{em}}(K) &\equiv \bar{\mathcal{E}}_{\text{rad}}^{\text{em}}(K) - \bar{E}(K) \\ &= -\frac{N_1(4l_2 + 2 - N_2)}{(4l_1 + 1)(4l_2 + 1)} \left\{ \sum_{k>0} \left\{ \begin{matrix} l_1 & l_1 & k \\ l_2 & l_2 & 1 \end{matrix} \right\} \right. \\ &\quad \times \langle l_1 \| C^{(k)} \| l_1 \rangle \langle l_2 \| C^{(k)} \| l_2 \rangle F^k(n_1 l_1, n_2 l_2) \\ &\quad \left. + \sum_k (-1)^k \left[\frac{2}{3} \delta(k, 1) - \frac{1}{2(2l_1 + 1)(2l_2 + 1)} \right] \right. \\ &\quad \left. \times \langle l_1 \| C^{(k)} \| l_2 \rangle^2 G^k(n_1 l_1, n_2 l_2) \right\}, \quad (29) \end{aligned}$$

$$\begin{aligned} \delta \mathcal{E}_{\text{rad}}^{\text{rec}}(K') &\equiv \bar{\mathcal{E}}_{\text{rad}}^{\text{rec}}(K') - \bar{E}(K') \\ &= -\frac{(4l_1 + 1 - N_1)(N_2 - 1)}{(4l_1 + 1)(4l_2 + 1)} \left\{ \sum_{k>0} \left\{ \begin{matrix} l_1 & l_2 & k \\ l_2 & l_2 & 1 \end{matrix} \right\} \right. \\ &\quad \times \langle l_1 \| C^{(k)} \| l_1 \rangle \langle l_2 \| C^{(k)} \| l_2 \rangle F^k(n_1 l_1, n_2 l_2) \\ &\quad \left. + \sum_k (-1)^k \left[\frac{2}{3} \delta(k, 1) - \frac{1}{2(2l_1 + 1)(2l_2 + 1)} \right] \right. \\ &\quad \left. \times \langle l_1 \| C^{(k)} \| l_2 \rangle^2 G^k(n_1 l_1, n_2 l_2) \right\}. \quad (30) \end{aligned}$$

It follows from Eq. (29) that the average energy of the emissive zone equals to the average energy of the initial configuration only for these transitions:

$$K_0 n_1 l_1^{N_1} n_2 l_2^{4l_2+2} \rightarrow K_0 n_1 l_1^{N_1+1} n_2 l_2^{4l_2+1}, \quad (31)$$

$$K_0 n_2 l_2^{N_2} \rightarrow K_0 n_1 l_1 n_2 l_2^{N_2-1}, \quad (32)$$

where the passive shells contained in K_0 can be closed or open.

Similarly, the average energy of the receptive zone equals to the average energy of the final configuration for the following transitions:

$$K_0 n_1 l_1^{4l_1+1} n_2 l_2^{N_2} \rightarrow K_0 n_1 l_1^{4l_1+2} n_2 l_2^{N_2-1}, \quad (33)$$

$$K_0 n_1 l_1^{N_1} n_2 l_2 \rightarrow K_0 n_1 l_1^{4l_1+1}. \quad (34)$$

The absolute value of the shift of the emissive zone increases with the number of electrons in the inner shell (N_1) and with the number of vacancies in the outer shell ($4l_2 + 2 - N_2$). On the contrary, $|\delta \mathcal{E}_{\text{rad}}^{\text{rec}}(K')|$ increases with the number of electrons ($N_2 - 1$) and with the number of vacancies in the inner shell ($4l_1 + 1 - N_1$).

The difference between the average energies of the zone and configuration becomes maximal for the transitions between neighbouring shells, when radial wave functions of the jumping electron in the initial and final configurations strongly overlap and the integrals F^k and G^k acquire large values. Usually in such a case the exchange Coulomb interaction between electrons plays more important role than the direct interaction. Especially at $n_1 = n_2$ and $l_2 = l_1 + 1$ the coefficient at the main exchange integral G^1 considerably exceeds the coefficient at the integral F^2 , thus the magnitude of the shift is mainly determined by its component with G^1 :

$$\begin{aligned} & \overline{\mathcal{E}}_{\text{rad}}^{\text{em}}(K_0 n l^{N_1} n(l+1)^{N_2}) \\ & \approx \overline{E}(K_0 n l^{N_1} n(l+1)^{N_2}) \\ & + \frac{N_1(4l+6-N_2)(16l^2+32l+9)}{6(2l+1)(2l+3)(4l+1)(4l+5)} \\ & \times G^1(nl, n(l+1)), \end{aligned} \quad (35)$$

$$\begin{aligned} & \overline{\mathcal{E}}_{\text{rad}}^{\text{rec}}(K_0 n l^{N_1+1} n(l+1)^{N_2-1}) \\ & \approx \overline{E}(K_0 n l^{N_1+1} n(l+1)^{N_2-1}) \\ & - \frac{(4l+1-N_1)(N_2-1)(16l^2+32l+9)}{6(2l+1)(2l+3)(4l+1)(4l+5)} \\ & \times G^1(nl, n(l+1)). \end{aligned} \quad (36)$$

Consequently, the average energy of the emissive zone usually increases with respect to the average energy of the initial configuration. It is related with the existence of two level groups caused by the Coulomb exchange interaction – only the levels of the upper group mainly participate in the transitions [96]. The shift of the receptive zone also tends to be positive.

The shift of the emissive zone obtains the maximal value, sometimes exceeding 20 eV, for the transitions

$$K_0 n l^{4l+1} n(l+1) \rightarrow K_0 n l^{4l+2}. \quad (37)$$

The maximal absolute value of the shift of the receptive zone is attained for the transitions

$$K_0 n l^0 n(l+1)^{4(l+1)+2} \rightarrow K_0 n l n(l+1)^{4(l+1)+1}. \quad (38)$$

However, such configurations with the empty inner shell (except s^0 shell) are rather exotic.

Similar dependence of the shift between the average energies of the zone and the configuration on the numbers of electrons and vacancies in the subshells holds in the relativistic approximation, too. However, the single-configuration relativistic approximation takes less correlation effects than such a nonrelativistic approximation and it is often necessary to consider all the complex of relativistic configurations originating from the same nonrelativistic configuration. The characteristics of zones for the transitions between such complexes can also be derived [91]. When the coupling within a shell is closer to LS rather than to the jj scheme, it is useful to apply the expressions given above for the nonrelativistic approximation replacing its radial integrals by the corresponding combinations of relativistic integrals [97].

According to Eqs. (7), (8) and (24), (25), the shift $\partial \overline{E}(K - K')$ can be presented as

$$\begin{aligned} & \partial \overline{E}(K - K') \\ & = \overline{E}(K - K') - [\overline{E}(K) - \overline{E}(K')] \\ & = [\overline{\mathcal{E}}^{\text{em}}(K) - \overline{E}(K)] - [\overline{\mathcal{E}}^{\text{rec}}(K') - \overline{E}(K)]. \end{aligned} \quad (39)$$

This quantity for distant configurations is of the order of several eV, but for the transitions between the neighbouring configurations, especially for Eqs. (33), (34) when the shift of the receptive zone disappears, can play a rather important role.

By using in Eqs. (20), (21) the average energy and variance of zone instead of these characteristics for configurations, more exact estimations of the width of

energy levels interval involved in the transition are obtained. Also the coefficient a in Eq. (22) taking into account the energetically allowed part of the transitions between the overlapping configurations must be rewritten:

$$a = \int_{-\infty}^{\infty} \rho^{\text{em}}(E) \int_{-\infty}^E \rho^{\text{rec}}(E') dE dE'. \quad (40)$$

In a similar way the Auger zones are introduced and used [48]. The moments of the emissive and receptive zones, corresponding to the Auger transitions $K \rightarrow K'\varepsilon$, are defined by the distribution moments:

$$\alpha_k^{\text{em}}(K) = \frac{\sum_{\gamma} \langle K\gamma | H | K\gamma \rangle^k \sum_{\gamma'\gamma''} A(K\gamma \rightarrow K'\gamma'\varepsilon\gamma'')}{A(K \rightarrow K'\varepsilon)}, \quad (41)$$

$$\alpha_k^{\text{rec}}(K') = \frac{\sum_{\gamma'} \langle K'\gamma' | H | K'\gamma' \rangle^k \sum_{\gamma\gamma''} A(K\gamma \rightarrow K'\gamma'\varepsilon\gamma'')}{A(K \rightarrow K'\varepsilon)}. \quad (42)$$

Here K, K' are the configurations of an atom and ion, ε is the energy of Auger electron, and γ' is a set of quantum numbers of this electron and of the whole system atom + free electron. $A(K \rightarrow K'\varepsilon)$ is the total transition rate. The expressions for the shift of the average energy of the Auger zone with respect to the average energy of the configuration were presented in [48].

The complex of programs for the calculation of global characteristics of spectra enables one to calculate the second moment of the Auger zones, too.

All the moments of the emissive zone coincide with the corresponding moments of the initial configuration K when it contains only one open shell (or sub-shell) involved in the considered Auger transitions:

$$K_0 \lambda_1^{N_1} \lambda_2^{\Omega_2} \lambda_3^{\Omega_3} \rightarrow K_0 \lambda_1^{N_1+1} \lambda_2^{\Omega_2-1} \lambda_3^{\Omega_3-1} \varepsilon \lambda, \quad (43)$$

$$K_0 \lambda_1^{N_1} \lambda_2^{\Omega_2} \rightarrow K_0 \lambda_1^{N_1+1} \lambda_2^{\Omega_2-2} \varepsilon \lambda, \quad (44)$$

where K_0 means all passive closed or open shells.

The receptive zone coincides with the final configuration of the ion for a considerably narrower class of transitions involving s electrons:

$$K_0 \lambda_1^{\Omega_1-1} s^2 \rightarrow K_0 \lambda_1^{\Omega_1} \varepsilon \lambda, \quad (45)$$

$$K_0 \lambda_1^{\Omega_1-1} s s' \rightarrow K_0 \lambda_1^{\Omega_1} \varepsilon \lambda. \quad (46)$$

In the case of the Coster–Kronig or super-Coster–Kronig transitions involving the neighbouring shells with the same principal quantum number the shift of the zone with respect to the corresponding configuration is also mainly determined by the Coulomb (in the relativistic approximation by Coulomb and Breit) interaction. The shift of the emissive zone is usually positive and it increases, when the number of electrons in the $\lambda_1^{N_1}$ shell increases and the number of electrons in the other active shell with the same principal quantum number decreases. The shift of the receptive zone has usually a smaller value. The average energy of Auger transitions between two configurations expressed in terms of average energies of zones differ mostly from the difference of the average energies of configurations for the transitions

$$Nl^{4l+1} n(l+1)^2 \rightarrow nl^{4l+2} \varepsilon l, \quad (47)$$

$$Nl^{4l+1} n(l+1)n_3 l_3^{N_3} \rightarrow nl^{4l+2} n_3 l_3^{N_3-1} \varepsilon l. \quad (48)$$

4. Calculation of spectra excited by a cascade of processes

4.1. Method of calculation

Relative total rates of transitions from the same initial configuration in percent give the branching ratios of its depopulation. These ratios calculated along all paths of a cascade present its branching scheme. By summing the percents at various ionization stages for all final configurations, from which further Auger decay is impossible energetically, the ratios of multicharged ions are obtained. The variation of these ratios with the energy of exciting particles gives the photoion-yield spectrum.

During the cascade complex Auger and characteristic emission spectra are generated. Due to a large natural width of lines they often coalesce into broad maxima, corresponding to the transitions between configurations or even complexes of configurations. Such maxima can be described using the global characteristics of spectra. If the maximum has a symmetric form, its envelope is described by a Gaussian function (23), where \bar{E} means the average energy and σ^2 the variance of transitions between two configurations. When the distribution of lines has significant asymmetry, the skewed Gaussian function must be used. It is obtained by multiplying the Gaussian function (23) by the factor

$$1 - \frac{1}{2} \kappa_1 \left[\frac{E - \bar{E}}{\sigma} - \frac{1}{3} \left(\frac{E - \bar{E}}{\sigma} \right)^3 \right]. \quad (49)$$

Here κ_1 is the coefficient of skewness [41]. It is expressed in terms of the third moment of spectrum μ_3 and the variance σ^2 :

$$\kappa_1 = \frac{\mu_3}{\sigma^3}. \quad (50)$$

By multiplying the distribution function by a population of the initial configuration and performing the summation of such functions for all transitions, which give the contribution in the considered energy interval, the envelope of the summary spectrum is obtained.

All main global characteristics of the emission and Auger spectra in nonrelativistic and relativistic approximations are calculated using the general computer code. The necessary algebraic expressions are derived by applying the algorithms of group-diagrammatic method [44,45] and then they are used in the calculations. Some formulae for the emission spectrum are presented in [38,41] and for the Auger spectrum in [42].

All radial integrals necessary for the applications presented in the following section were calculated by the pseudorelativistic Hartree–Fock method [98].

4.2. Production of multiply charged ions of lanthanides

Atoms of lanthanides with the $4f^N$ shell and other open shells in various configurations, which appear during the cascade, have a very large number of levels. Thus the detailed calculation of the cascade after the production of a vacancy in the inner shell is practically impossible. Additionally many overlapping configurations appear during the cascade and some transition arrays in lanthanides are distributed asymmetrically. This requires more accurate calculations using the global characteristics of zones and transition arrays.

Though various lanthanides have similar physical properties their photoion-yield spectra generated by photoabsorption in the region of $4d$ giant resonances show rather different behaviour: at the beginning of the group the triply charged ions have been mainly produced, while for the elements of the second part of the group the singly charged ions are predominant [8].

At the photon energies of 100–200 eV, used for the registration of spectra, the $4d$, $4f$, $5s$, and $5p$ shells can be effectively ionized. The Auger decay of these vacancies involves transitions between more than 100 configurations. They play very different roles: the total transition rates vary by more than five orders of magnitude.

Considering the Auger decay of each configuration, the weak transitions, which rate is smaller than 1% of the strongest transitions from this configuration, are omitted. The initial population of excited configurations with $4d^{-1}$, $4f^{-1}$, $5s^{-1}$, and $5p^{-1}$ vacancies was determined using the photoionization cross-sections calculated in the relativistic time-dependent local density approximation [7, 8].

The main part of the Auger cascade for Nd is shown in Fig. 1. This scheme demonstrates clearly that a large part of transitions takes place between the overlapping configurations and such transitions are only partially allowed. For them the total transition strength was diminished by the coefficient a , calculated according to Eq. (40). In the region of the giant photoabsorption the population of the initial states is mainly determined by the $4d$ and $4f$ photoionization (Fig. 2(d)). The Auger decay of $4d^{-1}$ vacancy including the shake-off transitions mainly produces triply (47%) and doubly (47%) charged ions. The decay of $5p^{-1}$ vacancy ends at the second ionization stage. This results in the predominance of Nd^{2+} ions during the cascade. All Nd^+ ions are formed by the production of $4f^{-1}$ vacancy, for which the Auger decay is forbidden energetically. A relatively small number of Nd^{4+} ions is produced essentially through the $4d^{-1} \rightarrow 5s^{-2} + e \rightarrow 5s^{-1}5p^{-1}6s^{-1} + 2e \rightarrow 5p^{-1}4f^{-1}6s^{-2} + 3e$ transitions. The contribution of the shake-off transitions is not very large, but when taking them into account the number of Nd^{3+} ions exceeds the number of Nd^{2+} ions at the maximal photoabsorption, and the qualitative correspondence to the experimental spectrum is obtained (Fig. 2).

In Dy the $4f$ orbital is essentially contracted compared to Nd and at the giant photoabsorption the $4d \rightarrow 4f$ photoexcitation becomes the main process. The decay of the $4d^9 4f^{11} 5d$ configuration by the super-Coster–Kronig transitions mainly populates the $4d^{10} 4f^9 5d$ configuration. Its levels are also populated effectively by the direct photoionization of the almost filled $4f^{10}$ shell. However, the Auger decay of the $4f^{-1}$ vacancy by transitions $4f^{-1} \rightarrow 6s^{-2} \epsilon l$ is allowed only to some levels of the partially overlapping configuration $4f^9 5d$. Thus, the photoion spectrum of Dy is dominated by Dy^+ production (Fig. 3). The number of Dy^{2+} ions is essentially increased by the shake-off process. For Dy even more than for Nd the accurate description of transitions between overlapping configurations is very important. Only using the distribution functions for zones (40) the correspondence to the experimental spectrum is obtained.

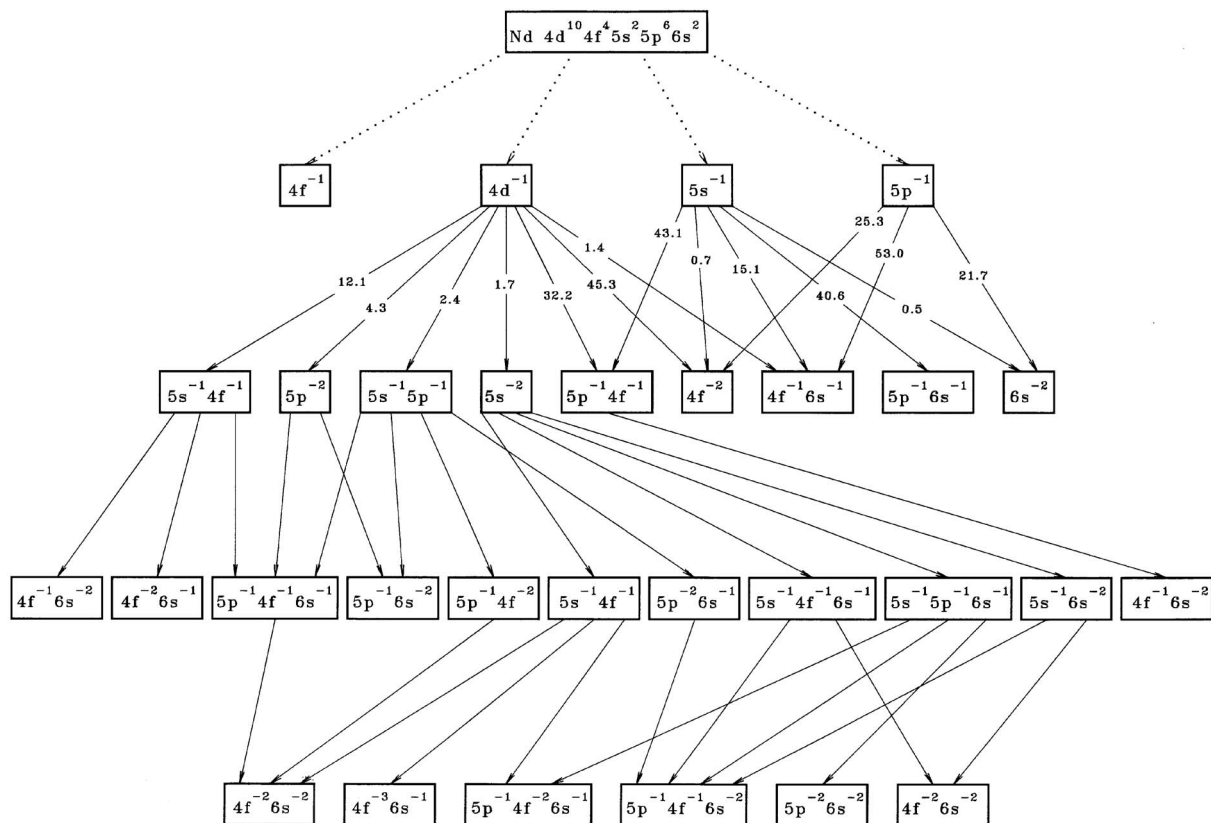


Fig. 1. The Auger cascade following photoionization of Nd atoms [64]: (\cdots) photoionization, ($-$) Auger transitions, ($- -$) partially allowed Auger transitions. Numbers at the arrows indicate the branching ratios in percent.

The photoion-yield spectra of Eu and Gd have their specific features related with the existence of the half-filled $4f^7$ shell, for these elements the correspondence to the experimental data has been obtained, too [64].

In [66] the distribution of the multiply charged ions of Eu after the resonant photoexcitation $3d_{3/2,5/2} \rightarrow 4f$ and $3d$ -ionization was calculated.

After the resonant excitation $3d_{5/2} \rightarrow 4f$ the distribution of ions reaches its maximum at Eu^{4+} (Fig. 4). After excitation $3d_{3/2} \rightarrow 4f$ the majority of ions are obtained with charge $q = 5+$ (Fig. 5). However, the ionization gives relatively more highly charged ions Eu^{6+} and Eu^{7+} , and it corresponds to the experimental data [99] measured using the time-of-flight mass spectrometer. Though the calculation reproduces qualitatively the charge distribution, in all cases the number of ions at low ionization stages is overestimated and at high ionization stages it is underestimated. The account of the shake-off process improves the correspondence to the experimental data, but not to a sufficient extent. The same discrepancy was noticed when considering the ratios of ions following the $3d$ ionization in xenon. One reason can be the correlation effects, especially in the decay of ns^{-1} and

np^{-1} vacancies at the presence of the other shells with the same principal quantum number. Some configuration mixing effects can be taken into account by global characteristics method, too [100], but the calculations become more complicated. Secondly, when considering the transitions between strongly overlapping configurations like one integral transition, they are treated to be forbidden when the average energy of the emission zone of the initial configuration exceeds the average energy of the receptive zone of the final configuration. However, transitions from some higher levels can remain allowed. It can be important, namely, at the ending stages of the cascades.

4.3. Use of global characteristics for the calculation of the Auger cascade spectrum

When the natural width of lines is rather large and the individual lines coalesce into broad maxima, corresponding to the transitions between configurations, the method of global characteristics can be applied not just for the investigation of cascade, but also for the calculation of the Auger cascade spectrum.

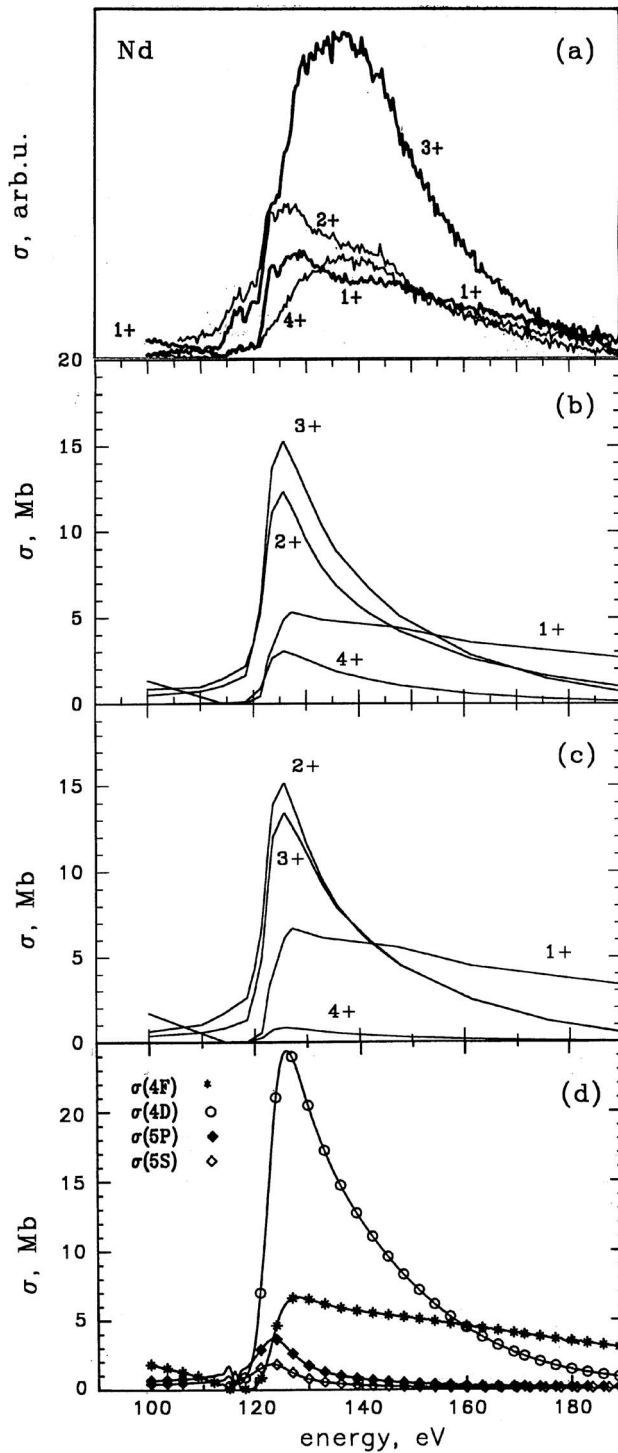


Fig. 2. Photoion-yield spectra of Nd^{i+} with $i = 1-4$: (a) experiment [7], (b) calculation taking into account the Auger and shake-off processes [64], (c) calculation without shake-off [64], and (d) partial photoionization cross-section σ_{nl} for the $4d$, $5s$, $5p$, and $4f$ shells using relativistic time-dependent local density approximation (RTDLA) [7].

As an example in Fig. 6 the Auger spectrum of Eu produced after $3d_{3/2} \rightarrow 4f$ photoexcitation is presented. The majority of the intensive maxima

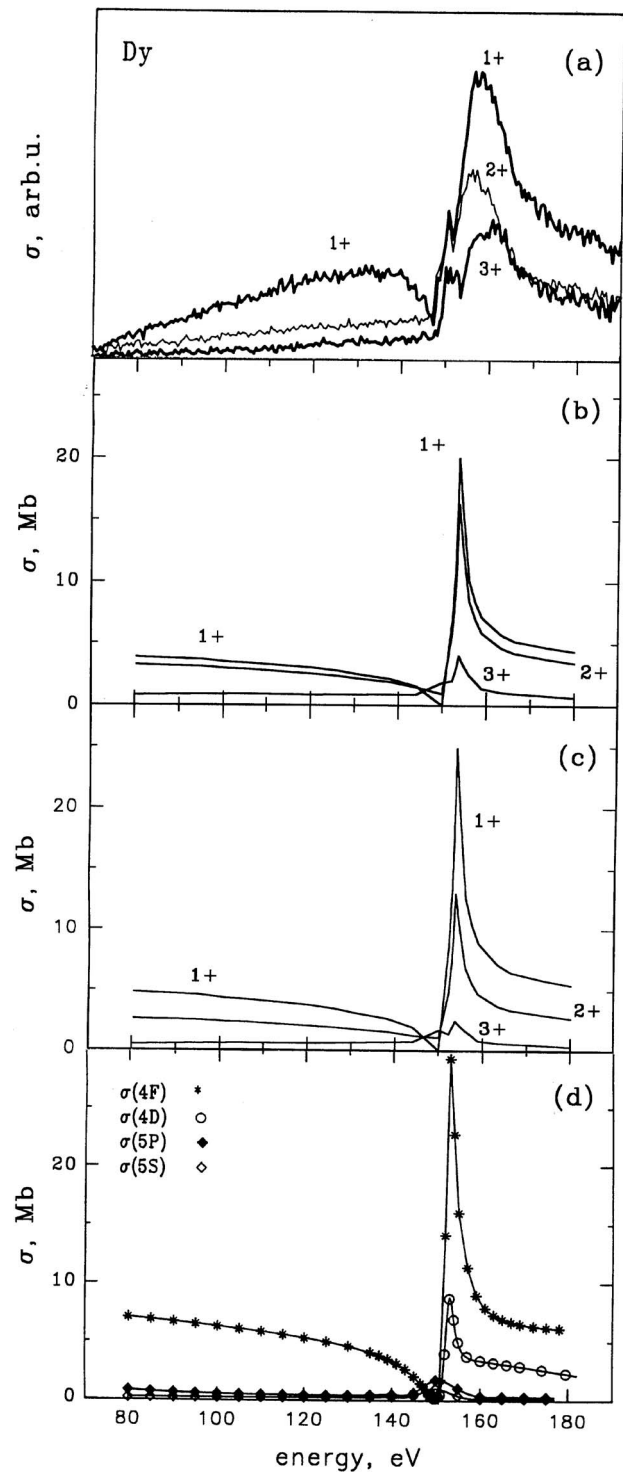


Fig. 3. Photoion-yield spectra of Dy^{i+} with $i = 1-3$: (a) experiment [8], (b) calculation taking into account the Auger and shake-off processes [64], (c) calculation without shake-off [64], and (d) partial photoionization cross-section σ_{nl} for the $4d$, $5s$, $5p$, and $4f$ shells using RTDLA [8].

corresponds to the direct Auger transitions from the initial excited configuration to the final configurations $4d^{-2}4f$, $4d^{-1}4f^{-1}$, $4p^{-1}4d^{-1}4f$, $4d^{-1}$, and

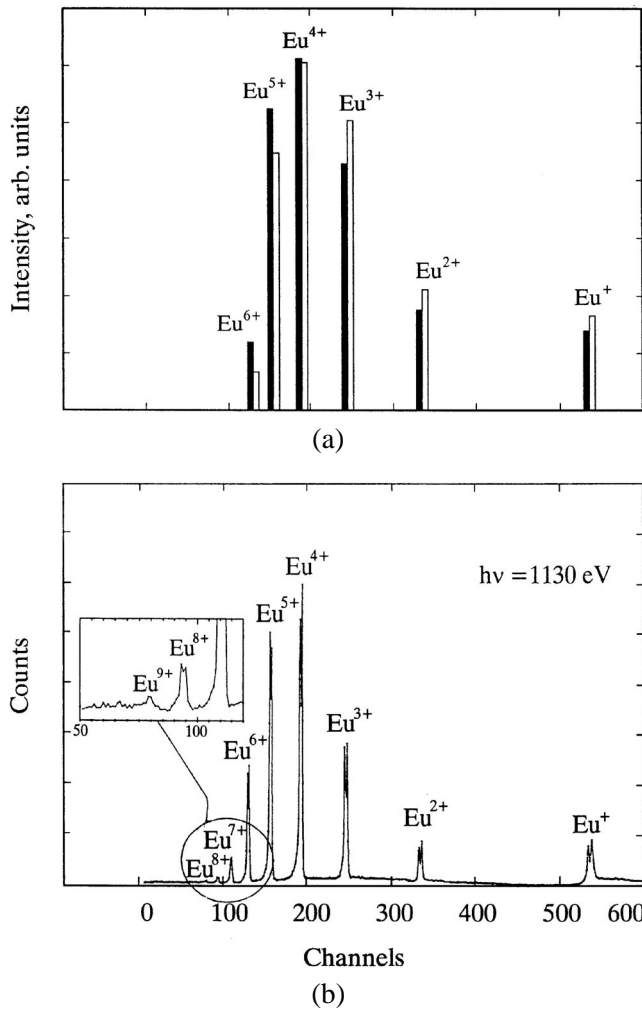


Fig. 4. Partial photoion-yield spectrum of Eu resulting from the resonant photoexcitation $3d_{5/2} \rightarrow 4f$: (a) calculation [64] (white columns – without shake-off transitions; black columns – the total spectrum), (b) experiment [99] taken at the photon energies $h\nu = 1130$ eV.

$4s^{-1}4d^{-1}4f$ (the number of vacancies and electrons are indicated with respect to the ground configuration Eu $4f^7$). However, with the relative probability equal to about 30% of the Coster–Kronig transitions, shifting of the vacancy from the $3d_{3/2}$ to the $3d_{5/2}$ subshell takes place. Thus, some additional maxima in the Auger spectrum can be attributed to the transitions from the $3d_{5/2}^{-1}4f$ configuration of Eu^+ to the final configurations $4d^{-2}$, $4f^{-2}$, and $4s^{-1}4d^{-1}$.

The method of global characteristics can be successfully used even for the interpretation of spectra having the fine structure which corresponds to the transitions between separate levels. Usually only a small main part of the cascade plays an essential role in the formation of the spectrum and the influence of many less probable transitions can be neglected. Thus, the ap-

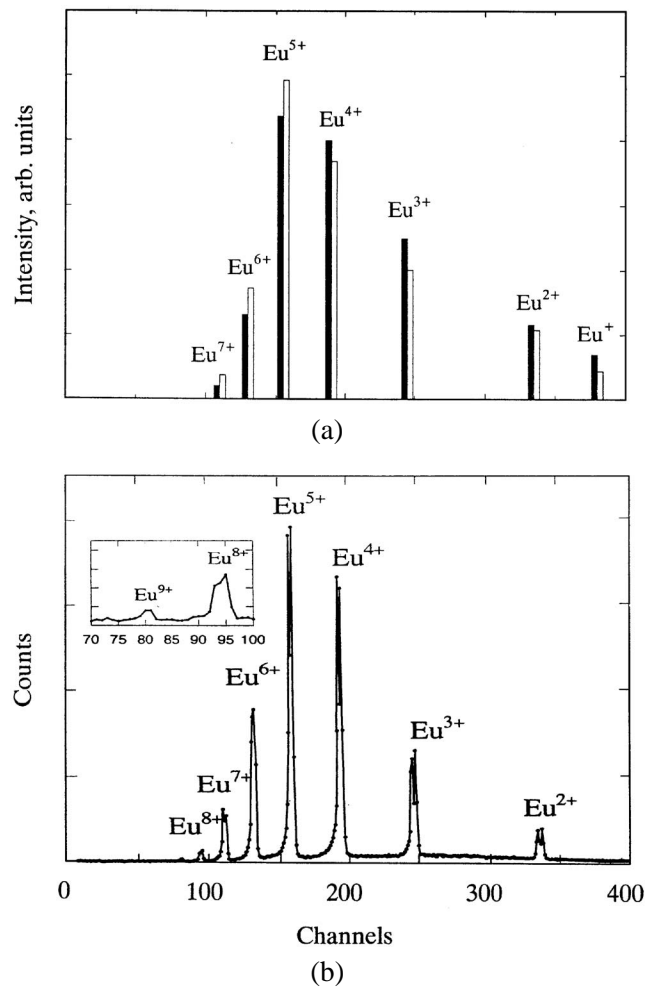


Fig. 5. Partial photoion-yield spectrum of Eu originating after the resonant photoexcitation $3d_{3/2} \rightarrow 4f$: (a) calculation [64] (black columns – *ab initio* result; white columns – the probabilities of $3d_{3/2}^{-1} \rightarrow 3d_{5/2}^{-1}nl^{-1}$ transitions multiplied by the empirical factor 3), (b) experiment [98] taken at the photon energies $h\nu = 1158.4$ eV.

proximate consideration of the whole cascade enables us to determine the most important processes and to perform only for them the detailed level-by-level calculations.

In Fig. 7, the Auger electron spectrum following the $3d$ ionization in xenon in the kinetic energy region of 8–40 eV is presented. The experimental spectrum was measured using the synchrotron radiation excitation with photon energy of 650 and 740 eV (below and above the $3d$ ionization threshold). By subtracting the first spectrum from the second one, the lines corresponding to the transitions due to the ionization of other shells were eliminated.

At first the calculation of the entire cascade after the production of $3d^{-1}$ vacancy was performed by the global characteristics method. The branching scheme

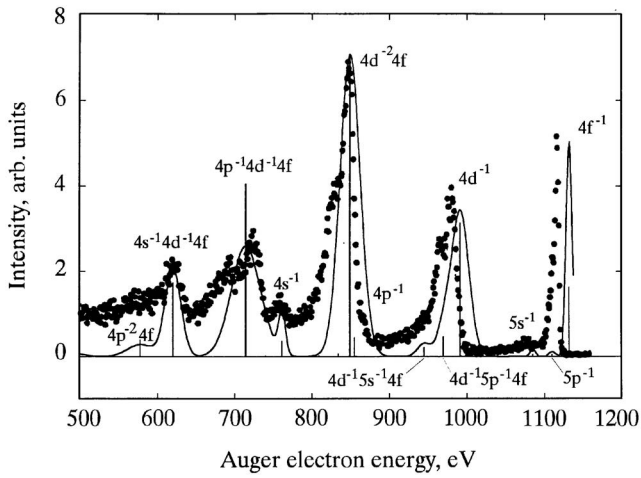


Fig. 6. The Auger spectrum of Eu due to decay of $3d_{5/2} \rightarrow 4f$ resonant photoexcitation: points are experimental data [101], thin solid curve gives the envelope of the calculated spectrum [66], vertical lines represent the total transition rates. The vacancies are indicated with respect to the ground configuration $4f^7 6s^2$.

of the most intense Auger transitions giving more than 1% contribution to the decay of initial states is shown. The obtained envelope reproduces the general distribution of the intensity in the spectrum. It is mainly determined by the following paths of Auger transitions:

$$3d^{-1} \rightarrow 4d^{-2} \rightarrow 4d^{-1}5p^{-2} \rightarrow 5p^{-4}, \quad (51)$$

$$3d^{-1} \rightarrow 4p^{-1}4d^{-1} \rightarrow 4d^{-2}5p^{-1} \rightarrow 4d^{-1}5p^{-3} \rightarrow 5p^{-5}. \quad (52)$$

The largest contributions indicated by labels 2, 8, 10, and 16 are given by the Auger transitions between the following configurations:

$$4d^{-1}5p^{-3} \rightarrow 5p^{-5},$$

$$4d^{-1}5p^{-2} \rightarrow 5p^{-4},$$

$$4d^{-2}5p^{-1} \rightarrow 4d^{-1}5p^{-3}, \quad \text{and}$$

$$4d^{-2} \rightarrow 4d^{-1}5p^{-2},$$

respectively.

The detailed calculations of the Auger transitions (51), (52) were carried out using the single-configuration pseudorelativistic Hartree–Fock method [98]. The calculated spectrum corresponds well to the experimental one and their comparison allows us to identify the main lines [32].

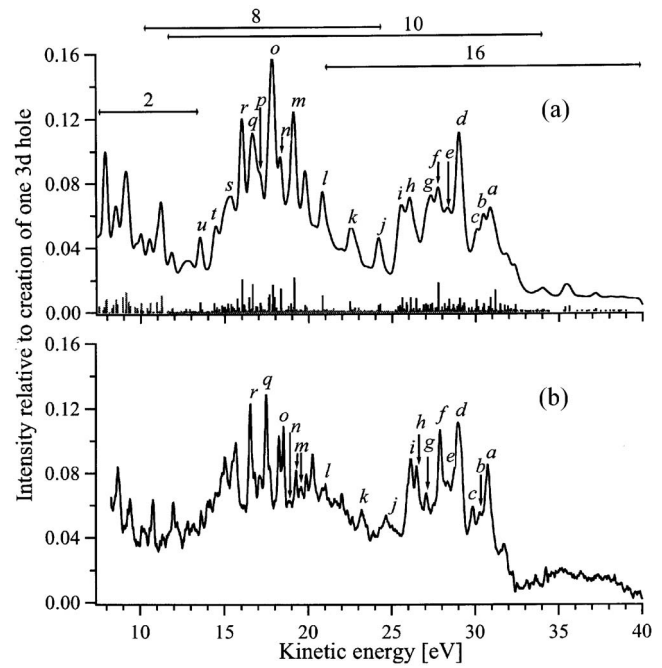


Fig. 7. The Auger cascade spectrum of Xe following the $3d$ ionization [32]: (a) experiment; (b) the envelope of the spectrum obtained by the global characteristics method (the most intense transitions lying in the energy region of 8–40 eV are indicated with labels); (c) the results of level-by-level calculations of the main part of the cascade. The kinetic energy regions of the Auger transitions are marked with horizontal arrows.

5. Conclusions

Cascades of processes following a vacancy creation in the inner electronic shell of an atom involve a large number of configurations with several open shells. Thus, the detailed level-by-level calculation of the entire cascade is usually impossible and even unnecessary. In the average atom model, the transitions between two configurations are treated as the integral transition with the total transition rate and the energy equal to the difference of the average energies of configurations. However, the transitions between the close-lying or overlapping configurations often play an important role in the cascade. Then besides the simplest global characteristics of the spectra – total transition rate, line strength, and the average energy of configuration – the supplementary characteristics such as the average energy and variance of transition array, characteristics of transition zones must be used. The existence of explicit expressions for these characteristics in the nonrelativistic and relativistic approximation and the realization of the general algorithm for their derivation in a computer code enable us to use effectively the global characteristics method for the description of the cascade and the af-

fect Auger or radiative spectra. Even when spectra have a fine structure, this method is useful for the preliminary investigation of the cascade to determine its main part, for which the detailed calculation can be performed.

Acknowledgement

We are grateful to Profs. H. Aksela, T. Nagata, and P. Zimmermann for the permission to reproduce their experimental results in this review.

References

- [1] F. Pleasonton and A.H. Snell, Proc. Roy. Soc. London Ser. A **241**, 141 (1957).
- [2] A.H. Snell, F. Pleasonton, and J.L. Need, Phys. Rev. **116**, 1548 (1959).
- [3] M.O. Krause, M.L. Vestal, W.H. Johnston, and T.A. Carlson, Phys. Rev. A **133**, 385 (1964).
- [4] T.A. Carlson and M.O. Krause, Phys. Rev. A **137**, 1655 (1965).
- [5] M.O. Krause and T.A. Carlson, Phys. Rev. **149**, 52 (1966); **158**, 18 (1967).
- [6] T.A. Carlson, W.E. Hunt, and M.O. Krause, Phys. Rev. **151**, 41 (1966).
- [7] Ch. Dzionk, W. Fiedler, M.V. Lucke, and P. Zimmermann, Phys. Rev. Lett. **62**, 878 (1989).
- [8] P. Zimmermann, Commun. At. Mol. Phys. **23**, 45 (1989).
- [9] T. Nagata et al., Physica Scripta **41**, 47 (1990).
- [10] W. Eberhardt, S. Bernstorff, H.M. Joachime, S.B. Whitsfield, and B. Crasemann, Phys. Rev. A **38**, 3908 (1988).
- [11] K. Ueda et al., J. Phys. B **24**, 605 (1991).
- [12] J. Doppelfeld et al., J. Phys. B **26**, 445 (1993).
- [13] F. von Busch, J. Doppelfeld, C. Günter, and H. Hartmann, J. Phys. B **27**, 2151 (1994).
- [14] D.W. Lindle et al., J. Electron. Spectrosc. Relat. Phenom. **67**, 373 (1994).
- [15] T. Luhmann, Ch. Gerth, M. Martins, M. Richter, and P. Zimmermann, Phys. Rev. Lett. **76**, 4320 (1996).
- [16] Y. Tamenori et al., J. Phys. B **35**, 2799 (2002).
- [17] O. Heber et al., Phys. Rev. A **39**, 4898 (1989).
- [18] V. Horvat et al., Nucl. Instrum. Methods **170**, 336 (2000).
- [19] M.N. Mirakhmedov and E.S. Parilis, J. Phys. B **23**, 821 (1990).
- [20] G. Omar and Y. Hahn, Phys. Rev. A **143**, 4695 (1991).
- [21] N. Vaecck et al., Physica Scripta **T95**, 68 (2001).
- [22] A.G. Kochur, J. Electron. Spectrosc. Relat. Phenom. **114**, 81 (2001).
- [23] A. Yutsis, J.B. Levinson, and V. Vanagas, *Mathematical Apparatus of the Theory of Angular Momentum* (National Science Foundation, Washington, 1962).
- [24] A. Jucys and A. Bandzaitis, *The Theory of Angular Momentum in Quantum Mechanics*, 2nd edn. (Mokslas, Vilnius, 1977) [in Russian].
- [25] A. Jucys and A. Savukynas, *The Mathematical Foundations of Atomic Theory* (Mintis, Vilnius, 1973) [in Russian].
- [26] E.J. McGuire, Phys. Rev. A **11**, 1889 (1975).
- [27] R. Karazija and S. Kučas, Liet. Fiz. Rink. **19**, 495 (1979) [Sov. Phys. – Collection **19**(4), 20 (1979)].
- [28] R.J. Karazija, J.J. Grudzinskas, S.A. Kučas, A.V. Karosienė, E.T. Verchovceva, and P.S. Pogrebniak, Opt. Spektrosk. (USSR) **57**, 395 (1984).
- [29] T. Kylli, H. Aksela, O.-P. Soiranen, A. Hiltunen, and S. Aksela, J. Phys. B **30**, 3647 (1997).
- [30] F. von Busch, U. Kuetgens, J. Doppelfeld, and S. Fritzsche, Phys. Rev. **59**, 2030 (1999).
- [31] S.-M. Huttula, S. Heinäsmäki, H. Aksela, E. Kukk, M. Hutulla, and S. Aksela, Phys. Rev. **67**, 052703 (2003).
- [32] V. Jonauskas, L. Partanen, S. Kučas, R. Karazija, M. Huttula, S. Aksela, and H. Aksela, J. Phys. B **36**, 4403 (2003).
- [33] M.N. Mirachmedov and E.S. Parilis, J. Phys. B **21**, 795 (1988).
- [34] T. Mukoyama, J. Phys. Soc. Jpn. **55**, 3054 (1986).
- [35] T. Mukoyama et al., J. Phys. B **20**, 4453 (1987).
- [36] A. El-Shemi, G. Lofty, and G. Zschornack, J. Phys. B **30**, 237 (1997).
- [37] V.L. Jacobs, J. Davis, B.S. Rozsnyai, and J.W. Cooper, Phys. Rev. A **21**, 1917 (1980).
- [38] C. Bauche-Arnoult, J. Bauche, and M. Klapisch, Phys. Rev. **20**, 2424 (1979).
- [39] S. Kučas and R. Karazija, Physica Scripta **47**, 754 (1993).
- [40] V. Jonauskas, S. Kučas, and R. Karazija, Physica Scripta **67**, 208 (2003).
- [41] S. Kučas, V. Jonauskas, and R. Karazija, Physica Scripta **51**, 566 (1995).
- [42] S. Kučas, R. Karazija, and V. Jonauskas, Physica Scripta **52**, 639 (1995).
- [43] J.N. Ginnocchio, Phys. Rev. C **8**, 135 (1973).
- [44] R. Karazija, *Sums of Atomic Quantities and Mean Characteristics of Spectra* (Mokslas, Vilnius, 1991) [in Russian].
- [45] R. Karazija and S. Kučas, Lithuanian J. Phys. **35**, 155 (1995).
- [46] A.G. Kochur, A.I. Dudenko, V.L. Sukhorukov, and I.D. Petrov, J. Phys. B. **27**, 1709 (1994).
- [47] J. Bauche, C. Bauche-Arnoult, E. Luc-Koenig, J.-F. Wyart, and M. Klapisch, Phys. Rev. A **28**, 829 (1983).
- [48] V. Jonauskas, R. Karazija, and S. Kučas, J. Phys. B **30**, 4861 (1997).

- [49] D.V. Morgan, M. Seguston, and R.J. Bartlett, *Phys. Rev. A* **55**, 1113 (1997).
- [50] M.G. Opendak, *Astrophys. Space Science* **165**, 9 (1990).
- [51] E. Murakami, T. Hayaishi, A. Yagishita, and Y. Morioka, *Physica Scripta* **41**, 468 (1990).
- [52] A.G. Kochur, Y.B. Mitkina, *J. Phys. B* **32**, 141 (1999).
- [53] S. Brünken et al., *Phys. Rev. A* **65**, 042708 (2002).
- [54] J.C. Levin et al., *Phys. Rev. Lett.* **65**, 988 (1990).
- [55] T. Matsui et al., *J. Phys. B* **35**, 3069 (2002).
- [56] Y. Tamenori et al., *J. Phys. B* **37**, 117 (2004).
- [57] T. Tonuma et al., *J. Phys. B* **20**, L31 (1987).
- [58] B. Kämmerling, B. Krässig, and V. Schmidt, *J. Phys. B* **25**, 3621 (1992).
- [59] H. Tavara et al., *J. Phys. B* **25**, 1467 (1992).
- [60] N. Saito and I.H. Suzuki, *J. Phys. B* **25**, 1785 (1992).
- [61] D.M. Holland, K. Codling, J.B. West, and G.V. Marz, *J. Phys. B* **12**, 2465 (1979).
- [62] N. Saito and I.H. Suzuki, *Physica Scripta* **49**, 80 (1994).
- [63] A.G. Kochur, V.L. Sukhorukov, A.I. Dudenko, and P.V. Demekhin, *J. Phys. B* **28**, 387 (1995).
- [64] S. Kučas and R. Karazija, *J. Phys. B* **29**, 1467 (1996).
- [65] T.M. Kojima et al., *J. Phys. B* **31**, 1463 (1998).
- [66] V. Jonauskas, R. Karazija, and S. Kučas, *J. Electron. Spectrosc. Relat. Phenom.* **107**, 147 (2000).
- [67] B. Kanngiesser et al., *Phys. Rev. A* **68**, 022704 (2003).
- [68] Y. Itoh et al., *J. Phys. B* **28**, 4733 (1995).
- [69] T. Koizumi et al., *J. Phys. B* **28**, 609 (1995).
- [70] M. Martins, P. Sladeczek, and P. Zimmermann, *J. Phys. B* **29**, L745 (1996).
- [71] M. Martins, P. Sladeczek, K. Tiedke, and P. Zimmermann, *Phys. Rev. A* **56**, 1329 (1997).
- [72] J.W. Cooper, S.H. Southworth, M.A. MacDonald, and T. LeBrun, *Phys. Rev. A* **50**, 405 (1994).
- [73] A.G. Kochur and V.L. Sukhorukov, *J. Electron. Spectrosc. Relat. Phenom.* **76**, 325 (1995).
- [74] G.B. Armen, J.C. Levin, and I.A. Sellin, *Phys. Rev. A* **53**, 772 (1996).
- [75] U. Alkemper, J. Doppelfeld, and F. von Busch, *Phys. Rev. A* **56**, 2741 (1997).
- [76] F. von Busch, J. Doppelfeld, U. Alkemper, U. Kuetsgens, and S. Fritzsche, *J. Electron. Spectrosc. Relat. Phenom.* **93**, 1 (1998).
- [77] F. von Busch et al., *Physica Scripta* **T80**, 401 (1999).
- [78] M. Kitajima et al., *J. Phys. B* **35**, 3327 (2002).
- [79] S.B. Whitfield, G.B. Armen, R. Carr, J.C. Levin, and B. Crasemann, *Phys. Rev.* **37**, 419 (1988).
- [80] M.H. Chen et al., *Phys. Rev. A* **15**, 2312 (1977).
- [81] E.T. Verkhovtseva and P.S. Pogrebnjak, *J. Phys. B* **13**, 3535 (1980).
- [82] E.T. Verkhovtseva, E.V. Gnatenko, P.S. Pogrebnjak, and A.A. Tkachenko, *J. Phys. B* **19**, 2089 (1986).
- [83] A.G. Kochur, Y.B. Mitkina, and V.L. Sukhorukov, *J. Phys. B* **31**, 5293 (1998).
- [84] A.G. Kochur, V.L. Sukhorukov, and Y.B. Mitkina, *J. Phys. B* **33**, 2949 (2000).
- [85] O. Simsek, *J. Phys. B* **35**, 1045 (2002).
- [86] K. Ueda et al., *J. Phys. B* **33**, L475 (2000).
- [87] K. Ueda et al., *J. Phys. B* **34**, 107 (2001).
- [88] M. Kitajima et al., *J. Phys. B* **34**, 3829 (2001).
- [89] S.-M. Hutulla et al., *Phys. Rev. A* **63**, 032703 (2001).
- [90] R. Karazija, *Introduction to the Theory of X-Ray and Electronic Spectra of Free Atoms* (Plenum, New York, 1996).
- [91] V. Jonauskas, S. Kučas, and R. Karazija, *Phys. Rev. E* (submitted).
- [92] L. Armstrong, Jr., *J. Math. Phys.* **9**, 1083 (1968).
- [93] Z.B. Rudzikas, *Theoretical Atomic Spectroscopy* (Cambridge University Press, Cambridge, 1997).
- [94] R. Karazija, A. Udris, and J. Grudzinskas, *Liet. Fiz. Rink.* **15**, 527 (1975) [*Sov. Phys. – Collection* **15**(4), 17 (1975)].
- [95] O. Peyrusse, *J. Phys. B* **32**, 683 (1999).
- [96] S. Kučas and R. Karazija, *J. Phys. B* **24**, 2925 (1991).
- [97] V. Jonauskas and R. Karazija, *J. Math. Phys.* **44**, 1660 (2003).
- [98] R.D. Cowan, *The Theory of Atomic Structure and Spectra* (University of California, Berkeley, 1981).
- [99] T. Nagata (private communication).
- [100] S. Kučas, V. Jonauskas, and R. Karazija, *Physica Scripta* **55**, 667 (1997).
- [101] G. Kutluk et al., *Photon Factory Activity Report B* **15**, 3 (1997).

KASKADŲ ATOMUOSE TYRIMAS NAUDOJANTIS BENDROSIOMIS SPEKTRŲ CHARAKTERISTIKOMIS

R. Karazija, S. Kučas, V. Jonauskas

VU Teorinės fizikos ir astronomijos institutas, Vilnius, Lietuva

Santrauka

Sukūrus atomo vidiniame sluoksnyje vakansiją, vyksta radiacinių ir Auger šuolių kaskada. Jų metu atomas daug kartų autojonizuojasi. Kaskados tiriamos, registruojant jonų išėigos, emisijos ir Auger spektrus. Šioje apžvalgoje apibūdinami teoriniai kaskadų nagrinėjimo metodai. Kadangi kaskadoje dalyvauja šimtai ir net tūkstančiai konfigūracijų su keliais atvirais sluoksniais, tai detalūs skaičiavimai yra sunkiai įmanomi. Dažniausiai nagrinėjami šuoliai

ne tarp atskirų lygmenų, bet tarp konfigūracijų, naudojantis bendrosiomis spektrų charakteristikomis – vidutine energija ir sumine tikimybe. Tačiau, vykstant šuoliams tarp artimų arba persiklojančių konfigūracijų, reikia naudoti aukštesnius spektrų momentus – dispersiją bei asimetrijos koeficientą, kurių algebrinės išraiškos yra rastos tiek nereliatyvistiniu, tiek reliatyvistiniu artėjimais. Pateikti kaskadų lantanidų atomuose skaičiavimo rezultatai; jie palyginti su eksperimentiniais spektrų duomenimis.